



Assessment of frictional-bond strength at the interface of single SSF in cementitious composite and prediction of accompanying pressure of surrounding matrix

Amjad Khabaz

To cite this article: Amjad Khabaz (2022): Assessment of frictional-bond strength at the interface of single SSF in cementitious composite and prediction of accompanying pressure of surrounding matrix, Composite Interfaces, DOI: [10.1080/09276440.2021.2017229](https://doi.org/10.1080/09276440.2021.2017229)

To link to this article: <https://doi.org/10.1080/09276440.2021.2017229>



Published online: 05 Jan 2022.



Submit your article to this journal [↗](#)



Article views: 180




View related articles [↗](#)



View Crossmark data [↗](#)



Assessment of frictional-bond strength at the interface of single SSF in cementitious composite and prediction of accompanying pressure of surrounding matrix

Amjad Khabaz 

Civil Engineering Department, Faculty of Engineering, Hasan Kalyoncu University, Gaziantep, Turkey

ABSTRACT

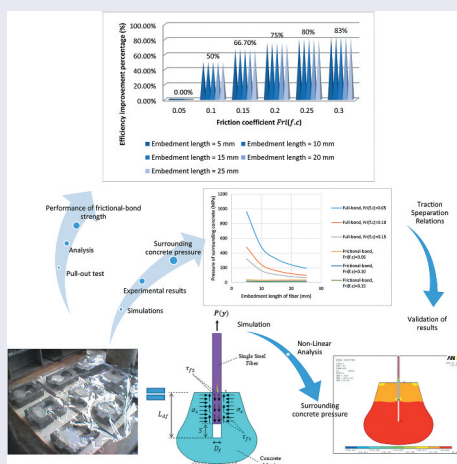
This paper deals with the study of bond in fiber-reinforced concrete composites and the effect of fiber/concrete interfacial friction on the fiber bond capacity. The paper presents the results of an experimental campaign including direct pull-out test of straight steel fiber-SSF embedded in concrete matrix, aimed at investigating the effect of some parameters, such as bonded length, yielding strength of steel fiber, fiber/concrete roughness, surrounding pressure of concrete matrix, and Poisson's ratio of concrete. Two analytical models based on the experimental results were proposed. Groups of single fiber embedded in concrete were prepared using different values of bonded length. The results showed that the frictional-bond strength, during fiber-slip stage, can be considered as constant despite changing the fiber embedment length. Furthermore, the SSF/concrete system can be considered as an elastic system, whereas the stress–displacement relation is semilinear. Finally, the results showed good improvements in the efficiency of frictional-bond strength when using fresh concrete with higher self-compacting, greater roughness at the interface of SSF/hardened-concrete, and fiber with lower yield strength. While no significant effect of Poisson's ratio on the frictional-bond strength was noticed.

ARTICLE HISTORY

Received 7 October 2021
Accepted 24 November 2021

KEYWORDS

Straight steel fiber-SSF; friction; fiber-slip; frictional-bond strength; interface; Poisson's ratio



1. Introduction

The strength of plain concrete under tensile stresses usually takes place around 10–12% compared to its compressive strength, and cracks are developed due to this weakness property [1–4].

When a structural element is prepared from plain concrete and loaded by a direct tensile force or bending moment, the concrete resists these applied loads by internal shear stress and normal stresses as tensile or compressive stresses [5–7].

In traditional reinforced concrete, steel rebars are usually used to resist the internal tensile stresses, and stirrups or bent bars are usually used to resist the shear stresses [8]. When plain concrete is subjected to tensile or shear stresses, initial cracks are developed, and sufficient post-cracking strength will be required to protect the concrete from brittle fracture [9,10].

In fiber-reinforced concrete (FRC) composites, the fiber is usually used to secure the required post-cracking strength, where the random distribution of fibers supports the concrete in all directions; consequently, improvements in composite strength are expected in all directions [11–14].

To obtain the required strength from the fibers inside cementitious composites, the bond strength between the fiber and the concrete should be sufficient at the interface of fiber to concrete [15–18].

When the fiber is subjected to tensile stresses inside concrete matrix, these tensile stresses are converted into shear stresses at the interface of fiber to concrete, then the bond strength starts to work as a guarantee to prevent the separation between the fiber and the concrete [19,20]. This separation at the interfaces may happen sometimes because of environmental reasons such as exposure to high temperature in summer seasons, especially in hot regions [21,22].

During the time of cement paste hydration, the binding quality is usually produced because of cement–water chemical reaction [23], which means a full-bond strength will be generated at the interface between the fiber and the concrete [24,25]. This interfacial full-bond strength should be sufficient with respect to the design requirements; otherwise, the composite will start in failure because of cracks development at the interfaces; these cracks can be considered as a warning for the service capacity, which means that the applied loads exceeded the design strength capacity [26,27].

To avoid the brittle fracture in the composite, the longer warning term is preferred, where the debonding stage term will be longer and the sliding performance of the fiber inside the concrete will be better [17,28]. The full-bond strength and the debonding performance are related to the chemical adhesion strength at the interface of fiber to concrete, where these types of bond strength should be designed according to assumed life service requirements of the composite [29].

If the applied tensile stresses on the fiber exceed the ultimate strength of the chemical full-bond strength, debonding behavior will happen at the interface, and after that the fiber tends to move inside the concrete by sliding behavior [30–34]. Then, the pressure of surrounding concrete and the roughness between the concrete and the fiber will work to prevent the fiber from sliding [35,36]. The friction at the interface converts the surrounding pressure of concrete into frictional shear stress [37,38].

To improve the frictional fiber-slip performance at the interface between the steel fiber and the concrete in FRC composites, deformed steel fibers can be used. Since the bond strength development is insufficient and premature pull-out failure with damages in the surrounding matrix by excessive anchorage effect, the limitations of using such deformed steel fibers were identified by some researchers [39]. To overcome the limitations of using highly deformed steel fibers in concrete matrix, new types of steel fibers were moderately deformed to prevent local stress concentration and surface-modified have been developed [40]. The pull-out resistance of smooth, straight steel fiber was better at inclined conditions in general [41], and according to this fact, Kim et al. [42] developed steel fibers having various curvatures, ranging from 0.02 to 0.10/mm, which prevent stress concentrations of drastic deformation like end hooks. The matrix damages were substantially mitigated during the fiber pull-out process, and the optimum type with a curvature of 0.04/mm led to a g -value of 109.3 kJ/m^3 , which is approximately 2.8 times higher than that of conventional straight fiber at the same fiber volume fraction of 1.5%. However, chemical treatment on the surface of steel fibers can be used as well to increase the roughness and interfacial frictional resistance with concrete matrix.

To evaluate the role of friction at the interface between the fiber and the matrix, establishing a contact model is helpful for researching the friction [43].

During the last years, micromechanical models for fiber-reinforced cementitious composite materials have gradually evolved in sophistication so that a structural performance-driven material design has been made possible [44]. The most crucial link between the properties of fiber, matrix, and fiber/matrix interface and that of a composite is the crack bridging stress–crack opening relation. Therefore, a reliable stress–strain relation of a composite based on a micromechanical model is needed in order to design a composite material that can meet the performance requirements of a structure. As discussed by [45], it was found that for nylon and polypropylene fibers, it was necessary to have an increasing interfacial shear stress with slippage distance (slip-hardening interface) in order to describe the experimental pull-out curves, while for steel fibers, a decreasing the interfacial shear stress with slippage distance was needed. According to [46] a Moire interferometry technique was used to measure the in-plane displacements around the continuous steel fiber/cement matrix interface, and the interface slip was calculated in addition to the interface shear stress, where the interface shear stress decayed with increasing value of the slip distance. Slip-dependent interface behavior has also been found in aligned continuous fiber-reinforced metal and ceramic matrix composites [47]. Several crack bridging models were developed as discussed in [48,49] for these aligned continuous fiber composites.

According to literature, despite of the big number of researches conducted on the pull-out mechanism of fiber to different types of surrounding matrix, it is obviously shown that the relations between the main parameters, which effect on the efficiency of the fiber/matrix frictional sliding, are still not completed, and also the question about how these parameters can be controlled properly to improve this efficiency is still not fully answered.

Therefore, the objective of this study is to (1) define the main factors, which may effect on the frictional-bond strength, such as the embedment length of fiber, the friction coefficient between the fiber and the concrete, the yield strength of fiber, the pressure of surrounding concrete, and Poisson's ratio of concrete; (2) derive the relationships

between these factors; (3) evaluate the role of each factor may effect on this frictional-sliding strength; (4) determine the main parameters that can be used to improve the efficiency of fiber-slip mechanism; and (5) assess the frictional-bond strength of SSF/concrete matrix under the defined parameters. To conduct such a study, two new analytical models have been developed. The first model is devoted to the fully bonded SSF/concrete matrix system, and the second model is devoted to the frictional sliding SSF/concrete matrix system. The results of these two models have been validated through finite element modeling and experimental pull-out tests as well.

The results of this study may add a worthy contribution to the industrial field through some applications such as development of devices for cracks development observation in FRC structures; early warning system of irregular live loads on buildings; consideration of new factors for concrete mix design that can be used to improve the efficiency of fiber/concrete system including the fiber type and its surface roughness; reduction of required quantity of cement as bonding material in concrete through controlling the morphology/topology contact surface between the fiber and the concrete in FRC structures, consequently reducing the cost of building construction; and improve the manufacturing properties of steel fibers in accordance with this study requirements with respect to the roughness and morphology of the steel fiber surface.

2. Materials and methods

2.1. Bond-slip mechanism

To describe the bond-slip mechanism of fiber/matrix system clearly, a typical curve of pull-out test of straight steel fiber-SSF in a cementitious composite is drawn as shown in [Figure 1](#), where the chemical full-bond strength at the interface controls the first stage of fiber pull-out mechanism under elastic behavior till reaching the critical load (P_{crit}), with fiber displacement equals (Δ_{crit}), (point 1). Then, the chemical bond yields under plastic behavior until reaching the ultimate full-bond strength point (point 2), which happens at a maximum pull-out load (P_{max}), where the fiber displacement is equal to (Δ_{max}). Then, the capacity of pull-out loads is getting down through nonlinear debonding behavior until reaching the full-debonding point (point 3), where the pull-out load is (P_0) and the fiber displacement equal to (Δ_0). At this point, the chemical bond is assumed to be fully broken overall the embedded length of the fiber. Then, the lateral pressure of concrete matrix around the fiber produces a new type of bond, which can be called as frictional-bond, where lateral pressure of surrounding concrete will be converted into an interfacial frictional-bond strength. This happens because of the roughness of fiber and concrete surfaces. When the fiber/matrix system is fully deboned, the fiber sliding stage will start, and the sliding–displacement will be measured along (S) axis, where at point 3 and before fiber sliding ($S = 0$), as shown in [Figure 1](#). During the fiber-sliding stage, which is considered as the final stage in the bond-slip mechanism, the frictional-bond strength works to resist the fiber from pulling out of the concrete until reaching the point of fully bond failure of fiber/concrete system (point 4).

For more understanding, and depending on the author research data, the bond-slip mechanism was described by monitoring the development of the applied pull-out load, $P(y)$, and the fiber displacement during all stages of pull-out test. This monitoring was

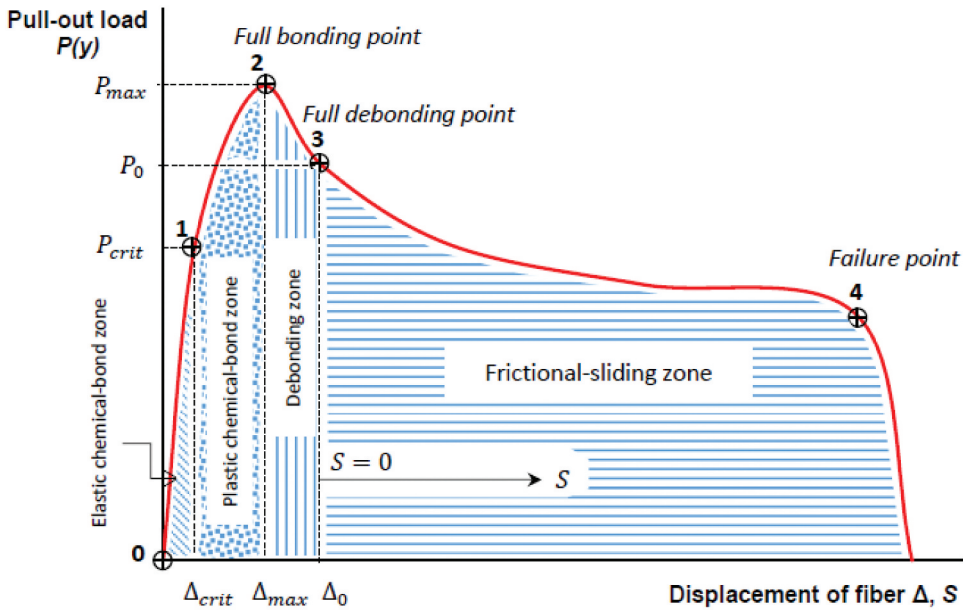


Figure 1. Typical curve of pull-out test of straight steel fiber-SSF in a cementitious composite.

done by using the results of computer simulations from previous works prepared by the author of this study. Therefore, we can say that bond between the fiber and the matrix usually starts as a perfect chemical bond; this bond works overall the embedded length of fiber in the concrete (l_{emb}), as shown in Figure 2a. In Figure 2, the contour plots of displacement vector sum are shown, and in this section there is no need to follow the precise values of the shown displacements, where these drawings are prepared to clarify the general deformed shape of fiber/matrix system during the different stages of pull-out test. The chemical bond, between the SSF and the concrete matrix, resists the pull-out loads until reaching the ultimate full-bonding point, where $P(y) = P_{max}$ and the fiber displacement is equal to (Δ_{max}), as shown in Figure 2b. After that a gradual separation between the fiber and the concrete grows at the interface through partial debonding behavior, with debonding length equal to (l_{debo}), as shown in Figure 2c, where the length of debonding zone expands gradually overall the embedded length of the fiber. While the capacity of pull-out load decreases until reaching the full-debonding point with fiber displacement equal to (Δ_0) and $P(y) = P_0$, with respect to the concrete matrix interface, as shown in Figure 2d. When the chemical bond is fully failed at the full-debonding point, the fiber tends to slide and pull out of the concrete matrix, and then a frictional shear stress is produced at the interface between the fiber and the concrete. This frictional shear stress happens because of the roughness between the surface of fiber and the surface of concrete, where the pressure of surrounding concrete is converted into an interfacial shear stress under the effect of friction, and this stress will be called as the frictional-bond strength.

The bond at the interface between the fiber and the concrete should meet all required conditions to activate the initial point of full-debonding, where the frictional-bond stresses can start in work. Therefore, the concrete mix, in this study, was designed taking

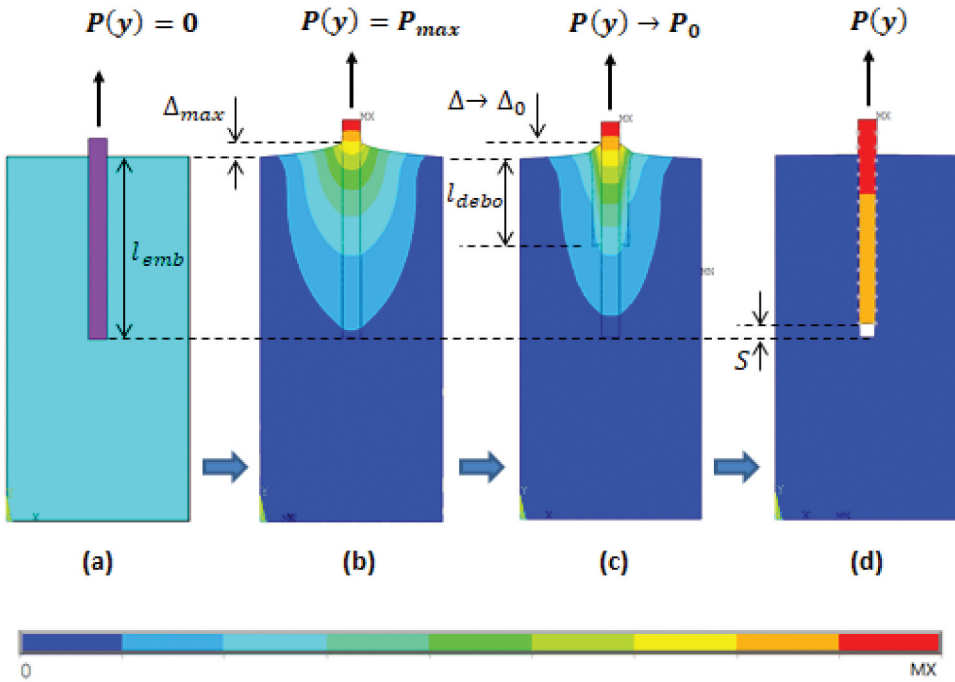


Figure 2. Bond-slip mechanism considering contour plot of displacement vector sum: (a) pre-critical; (b) full-bonding; (c) partial-debonding; (d) frictional-sliding phase.

into account the importance of bond properties after concrete hardening. These properties of bond are required to obtain sufficient adhesion between the particles of concrete after hardening, which is important to resist the development of cracks in the concrete during the pull out test.

2.2. Concrete mix properties and designation

The concrete mix was prepared using a laboratory trial method. The cement amount was designed to obtain sufficient full-bond strength between all concrete mix components, and the content of water was calculated to conduct a well hydration process for the cement paste, and to obtain an acceptable workability, where the ratio of water to cement was equal to 37%. Three types of sand aggregates were used; its sizes were ranged from 0 to 0.5 mm, from 0.3 to 2.5 mm, and from 2 to 4 mm, in addition to filler (dolomite powder) and microsilica, which is necessary to obtain an acceptable smoothness in the curve of graded aggregates. For improvement purposes in fresh concrete workability and air contents, in addition to adjustment of voids when the concrete becomes hard, two types of admixtures were used, SIKA EVO 26 and SIKA AER S. After mixing, the concrete mix was homogeneous with acceptable workability; the cone slump was equal to 7 cm. The density of fresh concrete was equal to 1955.3 kg/m³ (see Table 1). The modulus of elasticity of hardened concrete after 28 days was 30,000 MPa, and the compressive strength was 21 MPa. Also, Poisson's ratio was defined as 0.20.

Table 1. Concrete mix proportions.

Proportions of concrete mix	For 1 m ³
Cement II 42.5 A-V	575 kg
Water	213 l
Microsilica	49 kg
Dolomite powder filler	182 kg
Sand 0–0.5 mm	427 kg
Sand 0.3–2.5 mm	370 kg
Sand 2–4 mm	129 kg
Admixture SIKA EVO 26	8.7 l
Admixture SIKA AER S (10%)	1.6 l
Total weight of 1 m ³ concrete	1955.3 kg/m ³

2.3. SSF properties and chemical composition

The fiber in this research is a straight steel fiber-SSF with sufficient properties such as yield strength, elasticity modulus, Poisson's ratio, stiffness, and enough roughness at its external surfaces (see Figure 3). These properties are important to obtain a homogeneous work at the interfaces when the fiber is embedded into a concrete matrix in case of cementitious composite.

The main physical properties of the used fiber in this research are as follows:

The total length is 50 mm, the diameter is 0.8 mm, the yield strength 1200 MPa, the volume weight is 7850 kg/m³, and the modulus of elasticity is 200,000 MPa and Poisson's ratio is 0.28.

The chemical elements of steel fiber composition consist of carbon < 0.15, manganese < 0.95, silicium < 0.30, phosphate < 0.070, and sulfur < 0.050.

2.4. Experimental program

In this study, 15 experimental pull-out tests were conducted for different samples of single SSF embedded in concrete matrix. These samples have been divided into five groups, and each group consists of three samples. In the first group, the embedment length of fiber $L_{df} = 0.1L$, where L is the total length of fiber, which



Figure 3. Straight steel fiber-SSF.



Figure 4. Curing procedure of prepared samples.

is 50 mm. In the second group, the embedment length of fiber $L_{df} = 0.2L$. Then the embedment length of fiber $L_{df} = 0.3L$ in the third group, and the embedment length of fiber $L_{df} = 0.4L$ in the fourth group, and in the fifth group the embedment length of fiber $L_{df} = 0.5L$.

The method of curing was the moist-curing method, with room temperature 25 – 30, and humidity (H) rang $40\% < H < 80\%$, where after casting all samples are to be covered by a layer of soft nylon; in this case, the moisture of concrete will evaporate slowly and stronger concrete can be obtained (see Figure 4).

After 28 days, a pull-out test was conducted for each sample. The pull-out speed was maintained at 1 mm/min. Then records of force–displacement were taken to observe the mechanical behavior of fiber inside the concrete compared to the increment of pull-out tensile forces. Using these records, a curve of force–displacement can be drawn, then bonding and debonding points can be found for each sample, and frictional-interfacial stage can be shown as well, which is important to validate the analytical model of this study in addition to the governing equations.

2.5. Creation of analytical models

To derive the governing equations of full-bond strength and frictional-bond strength between the fiber and the concrete, we have to create two analytical models representing the interfacial shear stresses first in the stage of fully bonded fiber/matrix system and second in the frictional-sliding stage as mentioned before in Figure 2. These two analytical models should match the same real dimensions and properties of fiber and concrete materials, as what was used in the experimental program.

According to these assumptions, the first analytical model was created to describe the fully bonded fiber/matrix system as shown in Figure 5, and the second model was created to describe the sliding stage of fiber/matrix system as shown in Figure 6. In these two models, the concrete matrix is assumed to be fixed at the lower end,

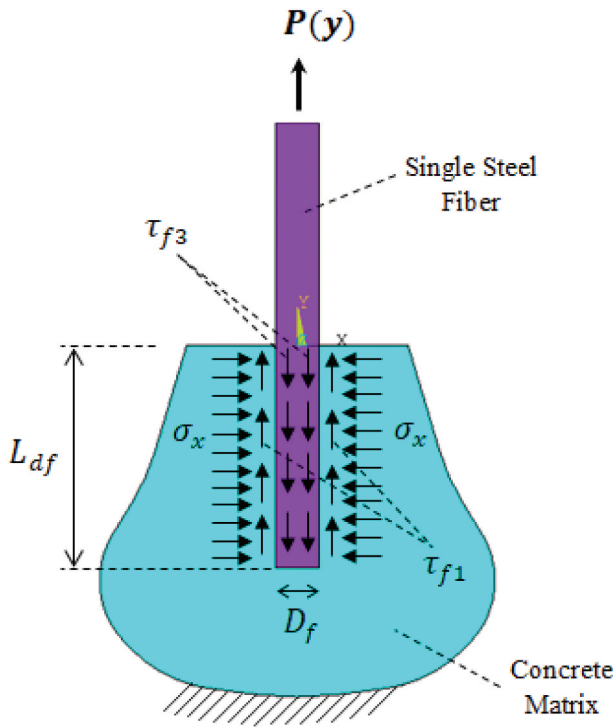


Figure 5. Fully bonded steel fiber/concrete matrix system 2D analytical model.

and the fiber is assumed to be free on the upper end. At the interface between the fiber and the concrete, the surface of fiber to matrix is assumed to be fully bonded in the first model, and in the second model the surface of fiber to matrix is assumed to be moveable under frictional sliding behavior.

In the first and second analytical models, $P(y)$ is assumed to be the applied tensile force on the free end of the fiber. In the first model, where the system of fiber/matrix is fully bonded, the equilibrium will be satisfied between the act force and the reaction. Therefore, the tensile force and the reaction at the fixed end of the concrete matrix will be in the same magnitude and opposite direction. In the second model, where the system of fiber/matrix is frictional sliding, the equilibrium will not be satisfied between the act force and the reaction, because of fiber pull-out movement upward. Therefore, during the sliding stage, the magnitude of the applied tensile force will be always greater than the reaction at the fixed end of the concrete matrix.

The concrete around the fiber will push the fiber by a surrounding pressure as normal stresses σ_x in x -direction to prevent the fiber from pulling out of the concrete. Therefore, this concrete pressure will be converted into interfacial-stress τ_{f1} on the side of concrete matrix, and τ_{f2} (in case of frictional-sliding system) or τ_{f3} (in case fully bonded system) on the side of fiber.

The diameter of fiber in all cases is considered as D_f , and the embedment length of the fiber inside the concrete matrix is considered as L_{df} .

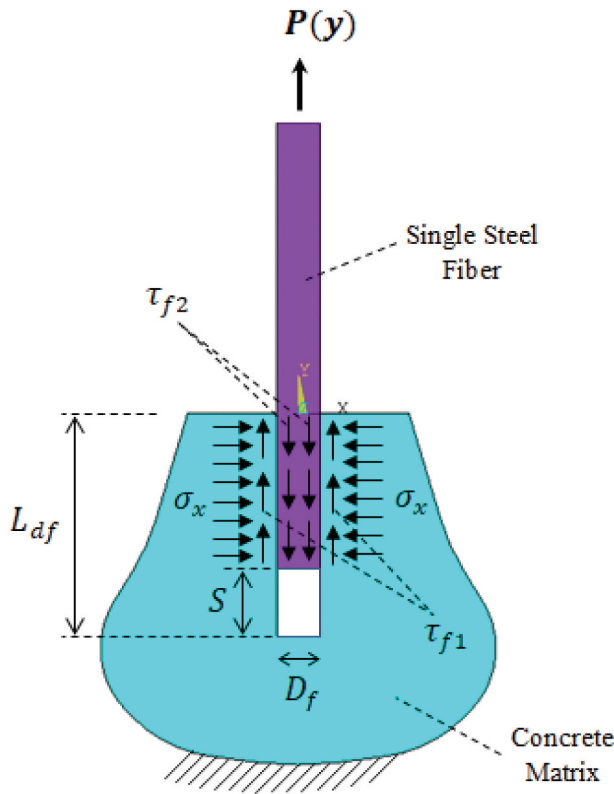


Figure 6. Frictional-sliding steel fiber/concrete matrix system 2D analytical model.

2.6. Derivation of governing equations

Returning to the analytical two models, when applying the tensile force $P(y)$, the frictional shear stress will be produced because of the roughness between the fiber and the concrete at the interface. This interfacial shear stress on concrete side τ_{f1} can be calculated as follows [50]:

$$\tau_{f1} = \sigma_x \times Fri_{(f.c)} \quad (1)$$

where $Fri_{(f.c)}$ is the coefficient of friction between the fiber and the concrete.

In case of fully bonded fiber/matrix system, if the embedded length of the straight steel fiber is greater than the development length, then the steel fiber may yield, leaving some length of the fiber inside the concrete. In this case, the required full-bond strength on the fiber surface τ_{f3} can be found theoretically depending on the principle of steel fiber development length L_{df} , as discussed in [51]. The steel fiber development length can be found using Equation (2) in terms of fiber diameter and steel fiber yield as follows:

$$L_{df} = \frac{D_f \times f_y}{4 \times \tau_{f3}} \quad (2)$$

where f_y is the yield strength of steel fiber.

Rearranging Equation (2) will give a suitable shape of an equation that can be used to calculate the full-bond strength, τ_{f3} , theoretically as follows:

$$\tau_{f3} = \frac{D_f \times f_y}{4 \times L_{df}} \quad (3)$$

Experimentally, in the phase of fiber slippage, the fiber can undergo sliding with either slip-hardening, constant friction, or slip-softening effect, which can be characterized by the coefficient (β), as discussed in [52,53]. Therefore, fiber pull-out behavior during sliding phase could be grouped into three categories, namely, slip-hardening ($\beta > 0$), constant friction ($\beta = 0$) and slip-softening ($\beta < 0$). Slip-hardening occurs often with polymer fibers. Because they are less hard than the surrounding matrix, they are damaged and a jamming effect can take place inside the matrix. Whereas constant friction or slip-softening is often observed when the fiber hardness is higher than that of the surrounding matrix.

The pull-out force $P(y)$ can be expressed in terms of fiber slip (S) using Equation (4) as follows:

$$P(y) = \tau_{f2} \times \pi \times D_f \times \left[L_{df} + S \times \left(\beta \times \frac{L_{df}}{D_f} - 1 \right) \right] \quad (4)$$

According to literature, the hardness of material is referenced by its compressive strength; consequently, the higher the compressive strength, the harder the material. The compressive strength of normal concrete in this study is 21 MPa, while it is 1200 MPa for the steel fiber. This leads to that the steel fiber hardness is higher than that of the surrounding concrete matrix; therefore, it can be assumed that ($\beta = 0$) or constant friction behavior during sliding phase throughout the derivation of governing equations, which is evident from the pull-out curve provided in the manuscript. Therefore, the pull-out force $P(y)$ can be expressed in terms of fiber slip (S) using Equation (5) as follows:

$$P(y) = \tau_{f2} \times \pi \times D_f \times (L_{df} - S) \quad (5)$$

Consequently, the instant interfacial-shear stress on the fiber surface (τ_{f2}) can be considered as the frictional-bond strength, and it can be found experimentally during fiber slippage using Equation (6) as follows:

$$\tau_{f2} = \frac{P(y)}{\pi \times D_f \times (L_{df} - S)} \quad (6)$$

The maximum frictional-bond strength will be met when ($\tau_{f2} = \tau_{f2max}$), and this will be obtained at the onset of fiber slippage, when [$S = 0$ and $P(y) = P_0$] (see Figure 2). Therefore, the maximum frictional-bond strength can be found experimentally by using Equation (7) as follows:

$$\tau_{f2max} = \frac{P_0}{\pi \times D_f \times L_{df}} \quad (7)$$

During fiber-sliding stage, when the fiber is pulling out of the matrix, the interfacial shear stress on concrete side τ_{f1} will be smaller than the instant interfacial shear stress on fiber surface τ_{f2} , and we can write

$$\tau_{f1} < \tau_{f2} \quad (8)$$

In this case, if we substitute τ_{f1} and τ_{f2} in Equation (8) by Equations (1) and (6), the relation between the surrounding pressure of concrete matrix and the instant pull-out load can be expressed as follows, with respect to the friction coefficient $Fri_{(f.c)}$:

$$\sigma_x < \frac{P(y)}{\pi \times D_f \times (L_{df} - S) \times Fri_{(f.c)}} \quad (9)$$

To obtain maximum resistance against fiber sliding inside the concrete, the interfacial shear stress on concrete side τ_{f1} should be greater than the interfacial shear stress on fiber surface τ_{f2max} .

Therefore, we can write

$$\tau_{f1} \geq \tau_{f2max} \quad (10)$$

Substituting τ_{f1} and τ_{f2max} in Equation (10) by Equations (1) and (7) will give

$$\sigma_x \times Fri_{(f.c)} \geq \frac{P_0}{\pi \times D_f \times L_{df}} \quad (11)$$

In Equation (11), σ_x represents the maximum predicted pressure of the surrounding concrete on the fiber surface. Therefore, to obtain experimentally the maximum frictional resistance against fiber sliding in the matrix, the required surrounding concrete pressure on the fiber surface can be predicted using Equation (12) as follows:

$$\sigma_x(\text{experimentally}) = \frac{P_0}{\pi \times D_f \times L_{df} \times Fri_{(f.c)}} \quad (12)$$

Whereas the required surrounding concrete pressure on the fiber surface, in case of fully bonded fiber/matrix system, can be predicted theoretically according to Equation (13) as follows:

$$\sigma_x(\text{theoretically}) = \frac{D_f \times f_y}{4 \times L_{df} \times Fri_{(f.c)}} \quad (13)$$

When the concrete matrix behaves elastically, a linear relationship between stress and strain can be considered. This linear relationship between the stress and the strain in concrete is defined by Hook's law as in Equation (14), where ε_x is the strain of the matrix in x -direction and E is the elasticity modulus of concrete matrix:

$$\sigma_x = \varepsilon_x \times E \quad (14)$$

Assuming that the materials of steel fiber and concrete matrix are isotropic (no directional dependence), the stress and the strain in y and z directions will not be equal to zero:

$$(\varepsilon_y = \varepsilon_z \neq 0)$$

$$(\sigma_y = \sigma_z \neq 0)$$

In literature, shear modulus of a material (G) is defined by Equation (15):

$$G = \frac{E}{2(1 + \nu)} \quad (15)$$

In Equation (15), ν is Poisson's ratio, which can be found using Equation (16), where ε_y is the strain of the concrete matrix in y -direction:

$$\nu = \frac{\text{latralstrain}}{\text{axialstrain}} = -\frac{\varepsilon_x}{\varepsilon_y} \quad (16)$$

According to Equation (15), the modulus of elasticity (E) can be expressed by Equation (17):

$$E = 2 \times G \times (1 + \nu) \quad (17)$$

Substituting the modulus of elasticity (E), as written in Equation (17), in Equation (14) of the surrounding concrete pressure (σ_x) will lead to a relationship between the required surrounding concrete pressure and Poisson's ratio as expressed in Equation (18):

$$\sigma_x = 2 \times \varepsilon_x \times G \times (1 + \nu) \quad (18)$$

2.7. Finite element modeling (FEM)

To monitor the frictional-sliding zone in the pull-out mechanism, FEM was prepared using ANSYS software. The finite element model can be used to study the effect of materials' properties and dimensions on the frictional sliding behavior of the fiber/matrix system, such as the fiber embedment length, the yield strength of steel fiber, the friction coefficient at the interface between the fiber and the concrete, and the Poisson's ratio of the concrete matrix.

Accordingly, a 2D finite element model was prepared by using the same shape and geometries of the proposed analytical model in the theoretical part of this study, as shown previously in Figure 6. In the finite element modeling, the elasticity modulus of 30,000 MPa and Poisson's ratio of 0.20 were used to construct the mesh of concrete matrix. Whereas the elasticity modulus of 200,000 MPa and Poisson's ratio of 0.28 were used to construct the straight steel fiber. Furthermore, the connection between the concrete and the fiber was prepared as a line-to-line contact element, with friction coefficient at the interface in changeable values.

To reach the required results from the FEM, a virtual tensile force $P(y)$ should be applied at the free end of the fiber, and the concrete mesh should be fixed from movements at its ends as shown in Figure 7.

3. Results and discussion

3.1. Experimental results of pull-out test

The frictional behavior at the interface of fiber/concrete can be observed by applying pull-out test on the samples of five groups, which are prepared using different values of embedment length of single steel fiber as mentioned before in the experimental program

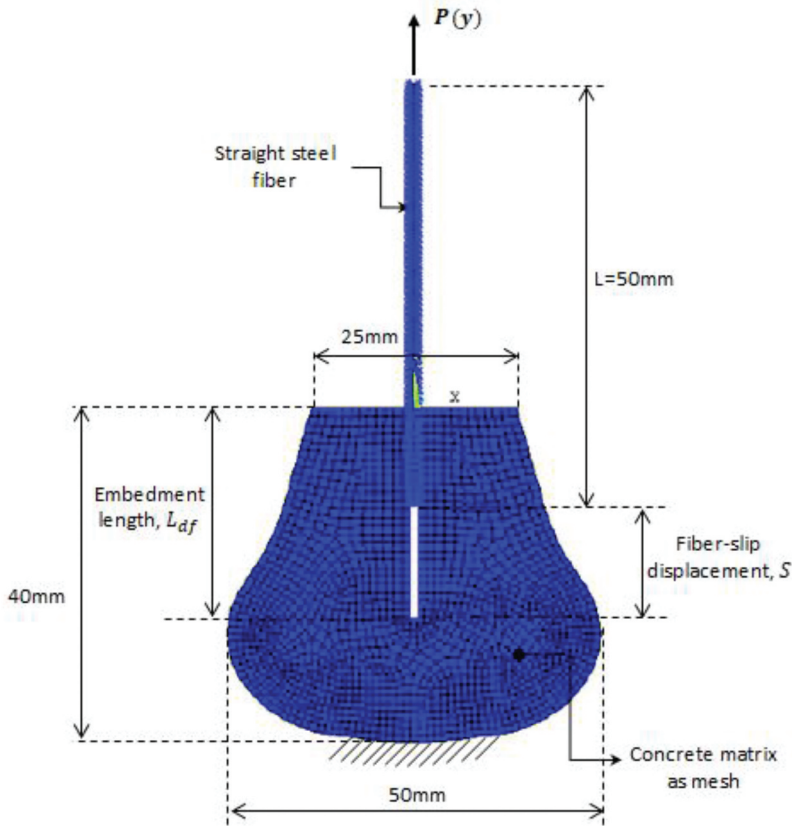


Figure 7. 2D finite element model represents the fiber/concrete system in the frictional-sliding stage.

section. The experimental curves of pull-out test showed the evolution of fiber displacement versus the evolution of pull-out force for each sample in each group, (see [Figures 8–12](#)).

Since the slope of force–displacement curve is constant (with angle α) in the zone of frictional sliding, as shown in [Figures 8–12](#), it can be concluded that assuming ($\beta = 0$) in the section of theoretical analysis in this study is validated experimentally. Consequently, it can be concluded that the relation of force–displacement is linear during the stage of fiber-slip.

3.2. Evaluation of bond strength and surrounding pressure

To evaluate the performance of the frictional-bond strength between the fiber and the concrete, with respect to different values of fiber embedment length (0.1 L, 0.2 L, 0.3 L, 0.4 L, 0.5 L), three values of friction coefficient $Fri_{(f.c)}$ will be used (0.05, 0.10, 0.15).

The maximum applied pull-out force P_0 at the tip of debonding zone can be found from the experimental pull-out test records after drawing the force–displacement curve for each case. Depending on P_0 , the frictional-bond strength τ_{f2max} can be found using Equation (7). Then, the accompanying pressure of surrounding concrete σ_x can be predicted experimentally by using Equation (12) (see [Table 2](#)).

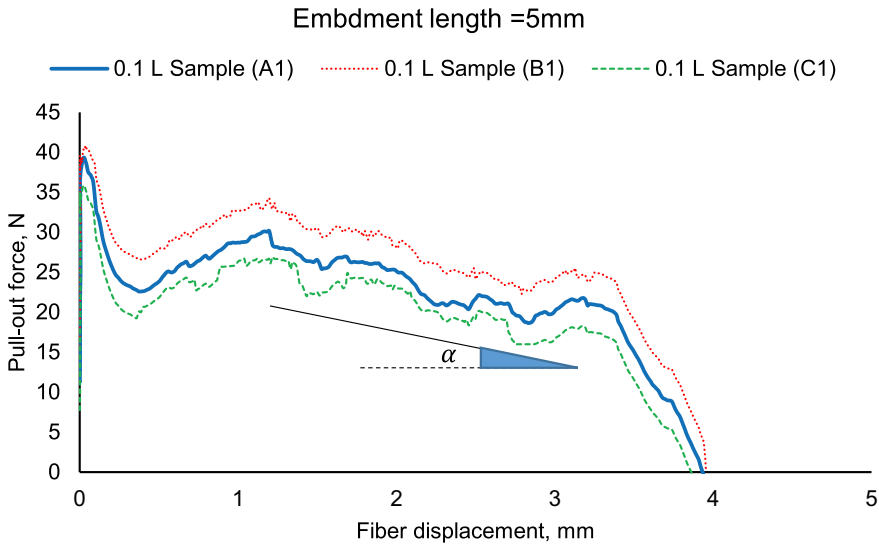


Figure 8. Experimental pull-out curve of single steel fiber in concrete matrix, $L_{df} = 0.1L$.

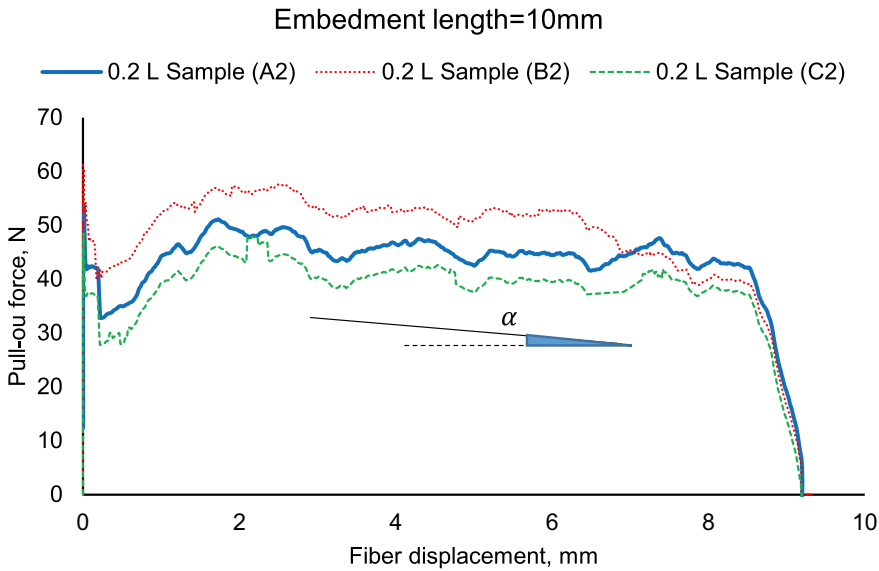


Figure 9. Experimental pull-out curve of single steel fiber in concrete matrix, $L_{df} = 0.2L$.

Theoretically, the full-bond strength τ_{f3} can be calculated using Equation (3), and the accompanying pressure of surrounding concrete σ_x in case of fully bonded steel fiber/concrete matrix system can be predicted using Equation (13) (see Table 3).

The evolution of the frictional-bond strength τ_{f2max} , compared to the fiber embedment length L_{df} , can be observed as shown in Figure 13, where it is clear that the frictional-bond strength can be considered as constant versus different values of fiber embedment length. While the full-bond strength of steel fiber/concrete matrix system is decreasing gradually when decreasing the value of fiber

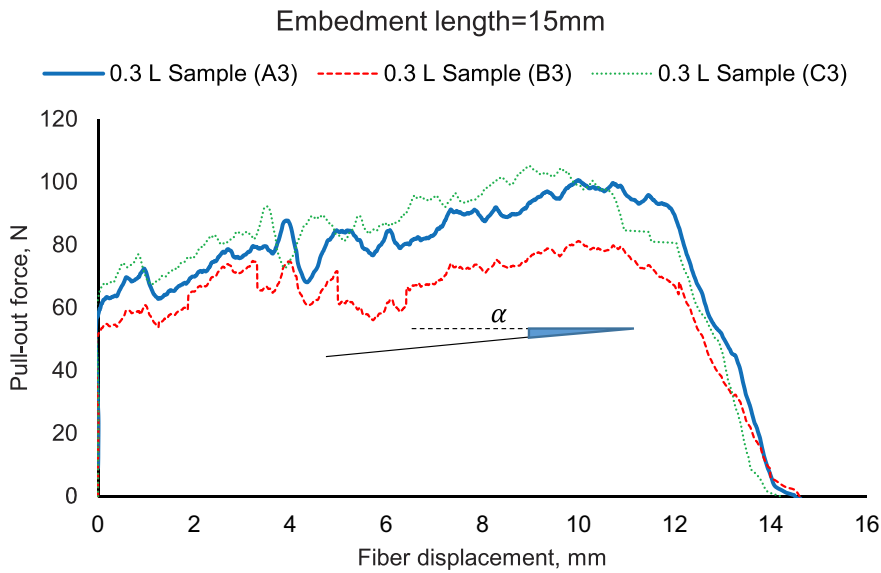


Figure 10. Experimental pull-out curve of single steel fiber in concrete matrix, $L_{df} = 0.3L$.

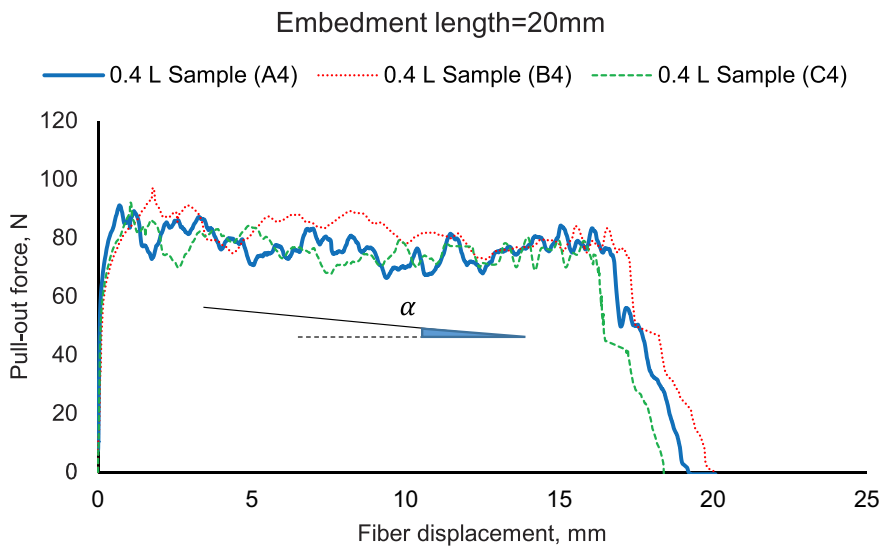


Figure 11. Experimental pull-out curve of single steel fiber in concrete matrix, $L_{df} = 0.4L$.

embedment length L_{df} . The results show big variations between the frictional-bond strength during the fiber-slip stage and the full-bond strength in case of fully bonded steel fiber/concrete matrix system. Since the full-bond strength was found by assuming an appropriate length for the steel fiber to develop its full yield strength, without failure in the bond strength between the fiber and the concrete, this means that the fiber plastic elongation will not be considered for bond strength lower than the full-bond strength (such as low values of frictional-bond strength, according to this study experimental records). Therefore, the plastic elongation of

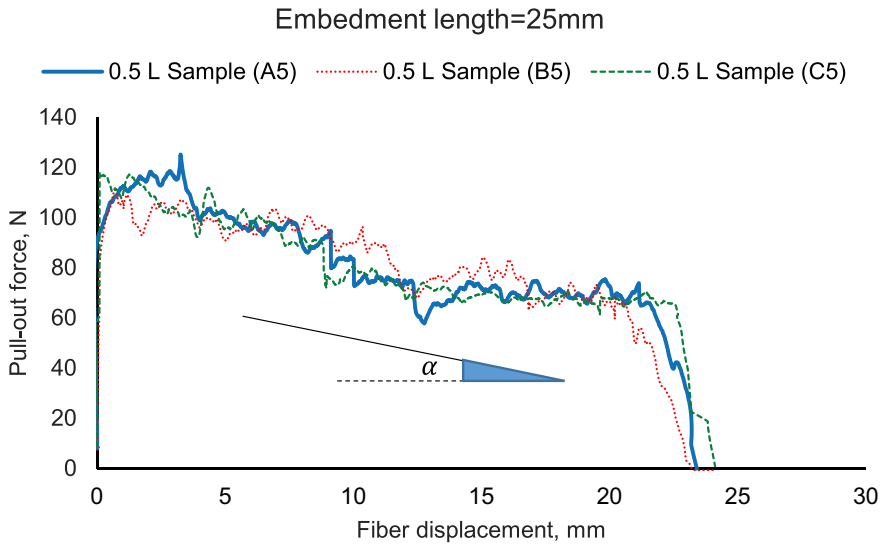


Figure 12. Experimental pull-out curve of single steel fiber in concrete matrix, $L_{df} = 0.5L$.

Table 2. Experimental frictional-bond strength and prediction of accompanying pressure of surrounding concrete at the interface between the fiber and the concrete using different values of friction coefficient $Fri_{(f,c)}$ and different values of fiber embedment length L_{df} .

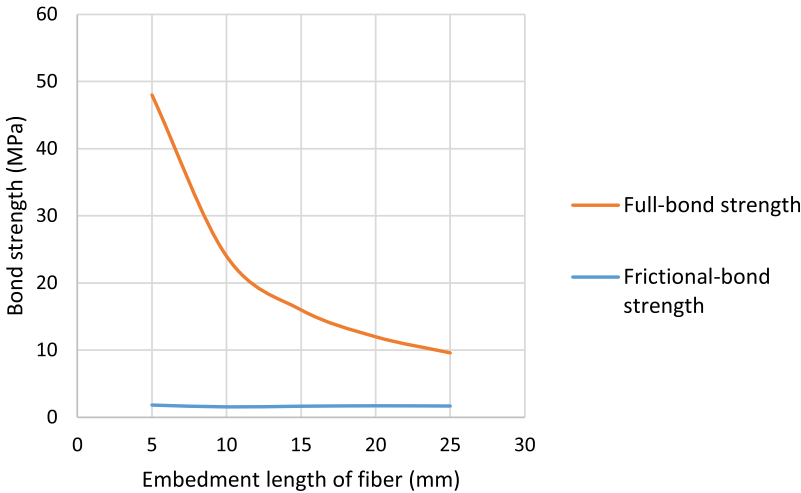
Embedment length, L_{df} (mm)	0.1 L = 5 mm	0.2 L = 10 mm	0.3 L = 15 mm	0.4 L = 20 mm	0.5 L = 25 mm
Pull-out load, P_0 (N)	23.0	39.2	62.5	86.5	106.3
Experimental frictional-bond strength, τ_{f2max} (MPa)	1.83	1.56	1.66	1.72	1.69
Accompanying pressure of surrounding concrete, σ_x (MPa) $Fri_{(f,c)} = 0.05$	36.61	31.19	33.16	34.42	33.84
Accompanying pressure of surrounding concrete, σ_x (MPa) $Fri_{(f,c)} = 0.10$	18.30	15.60	16.58	17.21	16.92
Accompanying pressure of surrounding concrete, σ_x (MPa) $Fri_{(f,c)} = 0.15$	12.20	10.40	11.05	11.47	11.28

steel fiber will not be met during fiber-slip stage in concrete matrix. Consequently, during the fiber-slip stage, the steel fiber/concrete matrix system can be considered as elastic system, and the stress–strain relation is linear.

During fiber-slip stage, assuming the matrix pressure as the required surrounding pressure to obtain the same value of frictional-bond strength, decreasing in the accompanying pressure of surrounding concrete matrix σ_x can be observed when applying a higher value of friction coefficient $Fri_{(f,c)}$, with respect to each value of fiber embedment length L_{df} , as shown in Figure 14. From this result, it can be concluded that in lightweight concrete, where the content of air voids is high, a higher value of friction coefficient is required to obtain the same frictional-bond strength; consequently, a larger roughness of fiber surface is required.

Table 3. Theoretical full-bond strength and prediction of accompanying pressure of surrounding concrete at the interface between the fiber and the concrete using different values of friction coefficient $Fri_{(f,c)}$ and different values of fiber embedment length L_{df} .

Embedment length, L_{df} (mm)	0.1 L = 5 mm	0.2 L = 10 mm	0.3 L = 15 mm	0.4 L = 20 mm	0.5 L = 25 mm
Yield strength of steel fiber, f_y (MPa)	1200	1200	1200	1200	1200
Theoretical full-bond strength, τ_{f3} (MPa)	48.00	24.00	16.00	12.00	9.60
Accompanying pressure of surrounding concrete, σ_x (MPa) $Fri_{(f,c)} = 0.05$	960	480	320	240	192
Accompanying pressure of surrounding concrete, σ_x (MPa) $Fri_{(f,c)} = 0.10$	480	240	160	120	96
Accompanying pressure of surrounding concrete, σ_x (MPa) $Fri_{(f,c)} = 0.15$	320	160	107	80	64

**Figure 13.** Evolution of frictional-bond strength τ_{f2max} and full-bond strength τ_{f3} versus different values of fiber embedment length L_{df} .

Also, during fiber-slip stage, the accompanying pressure of surrounding concrete matrix σ_x , can be considered as constant when using different values of fiber embedment length L_{df} , with respect to each value of friction coefficient $Fri_{(f,c)}$, as shown in Figure 15. While, in case of fully bonded fiber/matrix system, the accompanying pressure of surrounding concrete matrix was clearly related to the embedment length of the fiber L_{df} , and significant variations were observed when decreasing the value of the embedment length (see Figure 16).

According to the previous results, we can say that improving the self-compacting properties of fresh concrete may lead to a higher accompanying surrounding pressure; this will shift the tip of debonding zone to be placed at a point versus a greater value of fiber displacement, meaning the partial fiber stretching may add an additional contribution to the frictional-bond strength

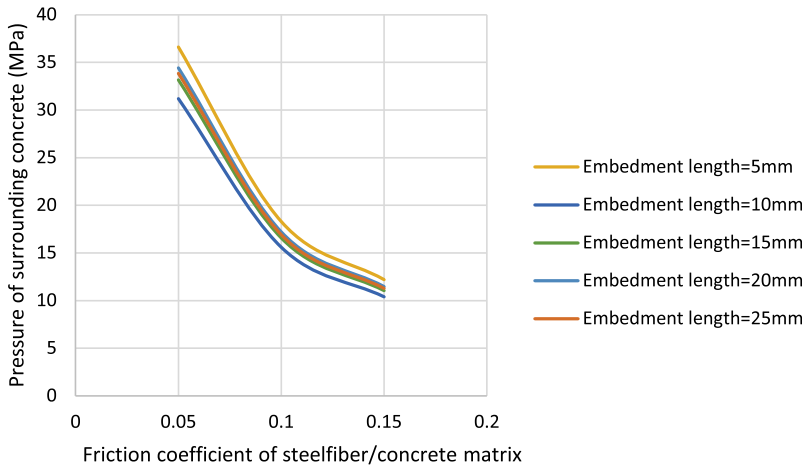


Figure 14. Accompanying pressure of surrounding concrete matrix σ_x in case of fiber-slip stage, with respect to the fiber/matrix friction coefficient $Fri_{(f,c)}$, using different values of fiber embedment length L_{df} .

Experimentally, it was noticed that the relation between the accompanying pressure of surrounding concrete, which is produced overall the embedded length of fiber because of the frictional sliding, and the evolution of fiber displacement is semilinear (see Table 4 and Figure 17). This semilinear behavior can be interpreted because of the changes in the morphology/topology of the fiber and concrete surfaces at the interface during the fiber-slip stage in the concrete.

Fiber-sliding behavior inside FRC composites can be monitored using numerical simulations as well. In the numerical simulations, different values of Poisson's ratio were used (0.16, 0.18, 0.20, 0.22, 0.24) for concrete mesh. The elasticity modulus of concrete mesh was assumed to be 30,000 MPa, and the elasticity modulus of straight steel fiber was assumed to be 200,000 MPa with fixed value of Poisson's ratio equal to 0.28. The connection between the concrete and the fiber was prepared as line-to-line contact element, while the friction factor at the interface was assumed to be 0.10. The embedment length of fiber in the concrete was assumed to be half of its total length, which is assumed 50 mm, and the diameter of fiber was assumed to be 0.8 mm. Simulations for different fiber displacements were prepared (3.6, 5.7, 13.7, 19.5, 21.6 mm); these displacements were selected according to experimental results, where these displacements follow the main points of force changes along the interface on the experimental curves. In the numerical simulations, the results showed semilinear distribution of deformation in x -direction in concrete along the interface between the fiber and the concrete (see Figure 18). Since all deformations usually happen due to the action of internal stresses in the same direction, this means there are semilinear distributed stresses act inside the concrete (which are x -component of internal normal stresses in concrete), and because of these stresses semilinear deformations have been produced in x -direction. This semilinear behavior can be interpreted as well because of the changes in the morphology/topology of the fiber and concrete surfaces at the interface during the fiber-slip stage in the concrete.

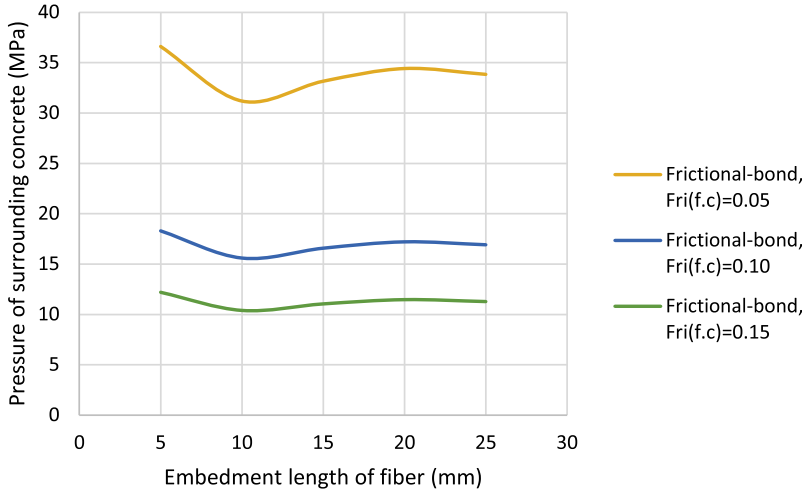


Figure 15. Accompanying pressure of surrounding concrete matrix σ_x in case of fiber-slip stage, with respect to the increment of fiber embedment length L_{df} , using different values of friction coefficient $Fri_{(f,c)}$ at the interface.

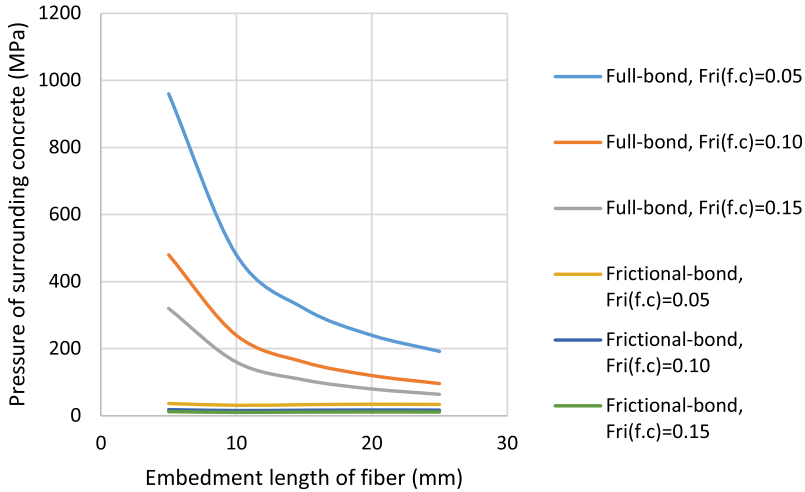


Figure 16. Accompanying pressure of surrounding concrete σ_x in case of frictional-bond compared to full-bond case, with respect to the increment of fiber embedment length L_{df} using different values of friction coefficient $Fri_{(f,c)}$ at the interface.

3.3. Impact of Poisson’s ratio on the frictional-bond strength

According to Equation (18) in Section 2.6, increasing Poisson’s ratio will increase the accompanying pressure of surrounding matrix (σ_x). Therefore, Poisson’s ratio may effect on the frictional-bond strength between the fiber and the concrete.

Since Poisson’s ratio represents the ratio between the transverse and longitudinal strain of the material, and the frictional-bond stress is produced from the effect of x -component of surrounding pressure on the interface, estimation of Poisson’s ratio impact is an important parameter for understanding whether this ratio will effect on the efficiency of frictional-bond strength or not.

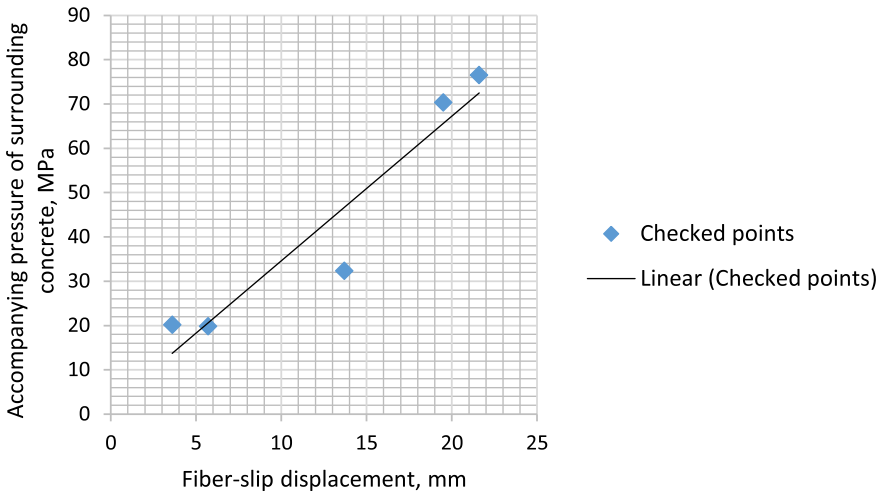


Figure 17. Evolution of the accompanying pressure of surrounding concrete σ_x along the remained part of fiber embedded length in the concrete during the fiber-slip stage, experimentally.

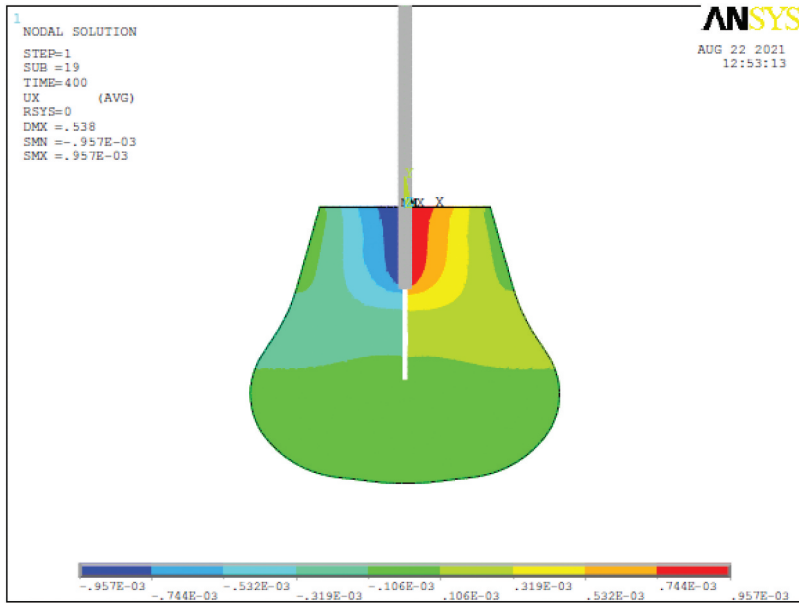
Accordingly, numerical simulations were used to conduct this study using different values of Poisson's ratio (0.16, 0.18, 0.20, 0.22, 0.24) for concrete mesh. In these simulations, the elasticity modulus of concrete mesh was 30,000 MPa, and the elasticity modulus for straight steel fiber was 200,000 MPa with a fixed value of Poisson's ratio equal to 0.28. The connection between the concrete and the fiber was prepared as line-to-line contact element, with friction coefficient at the interface equal to 0.10. The embedment length of fiber in the concrete was assumed to be half of its total length, and the total length was assumed to be 50 mm; the diameter of fiber was assumed to be 0.8 mm.

The simulation of each case of fiber-slip displacements (which were recorded in the experimental part of this study as mentioned in Table 4) was analyzed using nonlinear methods. The results of this analysis are shown in Table 5, where the maximum value of x -component of surrounding pressure in concrete has been monitored versus each value of Poisson's ratio (0.16, 0.18, 0.20, 0.22, 0.24).

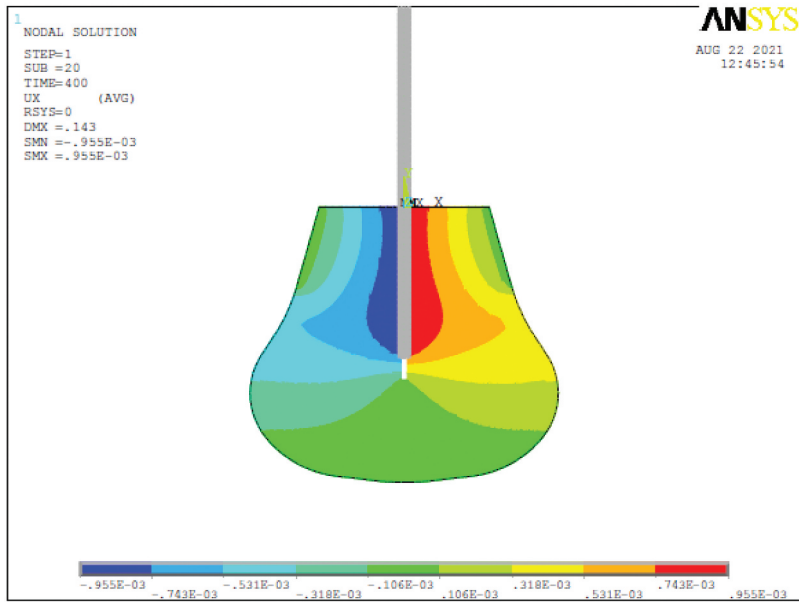
The results showed that Poisson's ratio of concrete does not effect on the frictional-bond strength at the interface between the fiber and the concrete, and no significant changes have been noticed on the x -component of surrounding pressure in concrete, which usually produce the frictional-bond strength at the interface (see Figures 19 and 20).

The results of computer simulations showed that the pressure of surrounding concrete is distributed uniformly overall the fiber embedment length during the fiber-slip stage (see Figure 20). This result is validated experimentally as shown in Figure 15. Consequently, assuming the surrounding pressure as uniform distributed pressure in the proposed analytical model can be validated as well.

Since the surrounding pressure is found in computer simulations as uniform distributed, the shear stress at the interface can be considered as uniform distributed as well. This result can be validated according to the experimental results as shown in Table 2 and Figure 13. Also, this result confirms the rightness of assuming uniform distribution of shear stress at the interface in the proposed analytical model.



(a)



(b)

Figure 18. Contour plot of deformed shape in x-direction for fiber displacements: (a) $S = 13.7$ mm, and (b) $S = 3.6$ mm.

3.4. Efficiency improvement of frictional-bond strength

To evaluate the efficiency of frictional-bond strength, we have to study the development of this efficiency compared to several changes in the value of the friction coefficient $Fri_{(f,c)}$ and in the embedment length of the fiber inside the concrete L_{df} . Therefore, the efficiency

Table 4. The instant value of the accompanying pressure of surrounding concrete σ_x along the remained part of fiber embedded length in the concrete during the fiber-slip stage, experimentally. $Fri_{(f,c)} = 0.10, D_f = 0.8\text{mm}, L_{df} = 25\text{mm}$

Fiber-slip displacement (mm)	3.6	5.7	13.7	19.5	21.6
(in)	0.143	0.224	0.538	0.770	0.852
The instant pull-out force $P(y)$ during fiber-slip stage (N)	108.36	95.88	91.85	97.16	65.37
The instant value of the accompanying pressure of surrounding concrete σ_x along the remained part of fiber embedded length in the concrete (MPa)	20.14	19.77	32.34	70.29	76.50

Table 5. Maximum values of surrounding pressure (at the interface) during frictional sliding of SSF inside concrete matrix, as numerical simulation.

Fiber-slip displacement (mm)	3.6	5.7	13.7	19.5	21.6
(in)	0.143	0.224	0.538	0.770	0.852
Poisson's ratio	Records of x -component of surrounding pressure in the concrete at the interface versus different values of Poisson's ratio, using numerical simulations (MPa)				
0.24	96.10	70.81	16.80	2.76	2.70
0.22	95.39	70.27	16.68	2.61	2.70
0.20	94.71	69.73	16.45	2.64	2.69
0.18	94.09	69.20	16.21	2.32	2.69
0.16	93.40	68.68	15.98	2.18	2.69

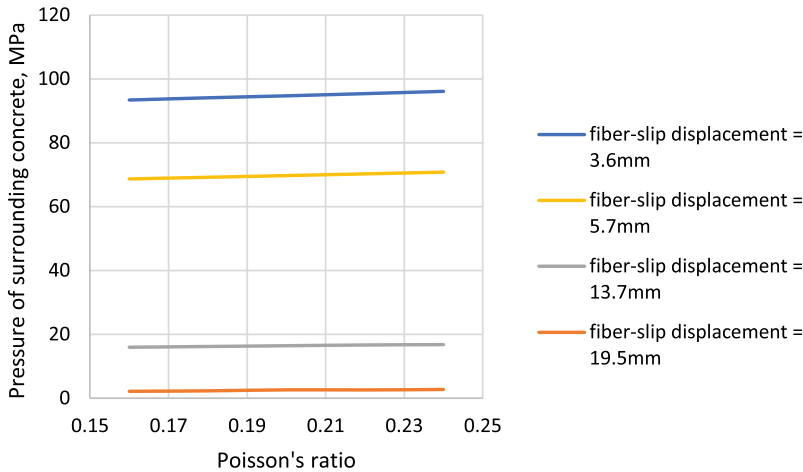


Figure 19. Records of surrounding concrete pressure at the interface versus different values of poisson's ratio, using numerical simulations.

improvement percentage can be estimated by using the results of the accompanying pressure of surrounding concrete σ_x for different values of friction coefficient $Fri_{(f,c)}$ and different values of fiber embedment length L_{df} as shown previously in Table 2. The surrounding pressure can be defined as the pressure of the fresh concrete around the fiber during the casting process, and since the frictional-bond strength equals the surrounding pressure times the friction coefficient between the fiber and the concrete, the lower value

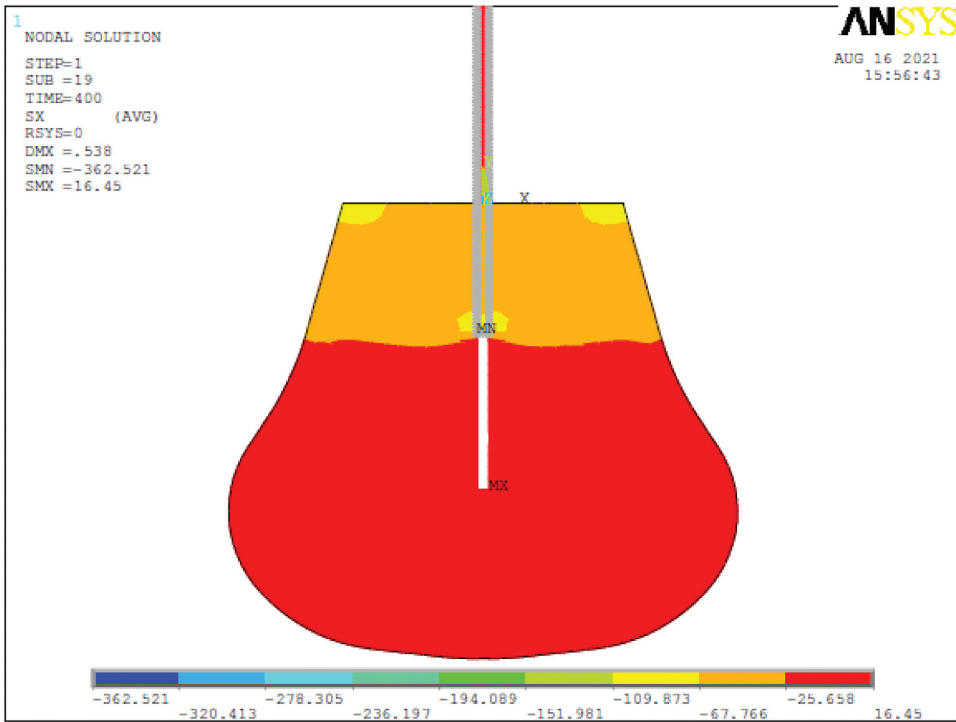


Figure 20. Monitoring of surrounding concrete pressure at the interface using Poisson’s ratio equals to 0.20 and fiber displacement equal to 13.7 mm.

of the accompanying pressure of surrounding concrete σ_x versus larger values of friction coefficient $Fri_{(f.c)}$ or embedment length L_{df} means that the same value of the frictional-bond strength can be obtained by a lower pressure from the fresh concrete. The lower pressure of fresh concrete means that the concrete mix might include a greater content of air voids, and this means a smaller contact area between the fiber and the concrete pieces at the interface. Consequently, the lower accompanying pressure of surrounding concrete, as hardened matrix, refers to that the efficiency of the frictional-bond strength is improved.

In case of fiber embedment length $L_{df} = 5mm$, if the friction coefficient $Fri_{(f.c)}$ increased from 0.05 to 0.10, the improvement percentage of the frictional-bond strength efficiency will equal to

$$\frac{|\sigma_{x(0.10)} - \sigma_{x(0.05)}|}{\sigma_{x(0.05)}} \times 100\% = \frac{|18.30(MPa) - 36.61(MPa)|}{36.61(MPa)} \times 100\% = 50\%$$

In case of fiber embedment length $L_{df} = 5mm$, if the friction coefficient $Fri_{(f.c)}$ increased from 0.05 to 0.15, the improvement percentage of the frictional-bond strength efficiency will equal to

$$\frac{|\sigma_{x(0.15)} - \sigma_{x(0.05)}|}{\sigma_{x(0.05)}} \times 100\% = \frac{|12.20(MPa) - 36.61(MPa)|}{36.61(MPa)} \times 100\% = 66.7\%$$

Table 6. Efficiency improvement percentage of frictional-bond strength.

Friction coefficient $Fri_{(f.c)}$		0.05 (reference)	0.10 (%)	0.15 (%)	0.20 (%)	0.25 (%)	0.30 (%)
Fiber embedment length L_{df} (mm)	5	–	50	66.7	75	80	83
	10	–	50	66.7	75	80	83
	15	–	50	66.7	75	80	83
	20	–	50	66.7	75	80	83
	25	–	50	66.7	75	80	83

By using the same way of calculations for greater values of fiber embedment length $L_{df} = 10\text{mm}$ and 15mm , the efficiency improvement percentage of the frictional-bond strength can be found as shown in Table 6, where the calculations extended including additional values of friction coefficient (0.20, 0.25, 0.30).

The evolution of the efficiency improvement parentage of frictional-bond strength can be observed clearly as shown in Figure 21. According to this figure, and whatever the value of fiber embedment length L_{df} , it can be noticed that the efficiency of frictional-bond strength was increased 50% in case of increasing the friction coefficient $Fri_{(f.c)}$ from 0.05 to 0.10 (what means increasing the friction coefficient by 100%), and the efficiency of frictional-bond strength was increased 66.7% in case of increasing the friction coefficient $Fri_{(f.c)}$ from 0.05 to 0.15 (what means increasing the friction coefficient by 200%). Whereas the efficiency of frictional-bond strength was increased (75%, 80%, 83%) in case of increasing the friction coefficient $Fri_{(f.c)}$ from 0.05 to (0.20, 0.25, 0.30) respectively. Therefore, it can be concluded that the effect of the friction coefficient $Fri_{(f.c)}$ on the efficiency of the frictional-bond strength is limited after exceeding the value of 0.10, and no significant improvements may be expected. This can be interpreted because of the

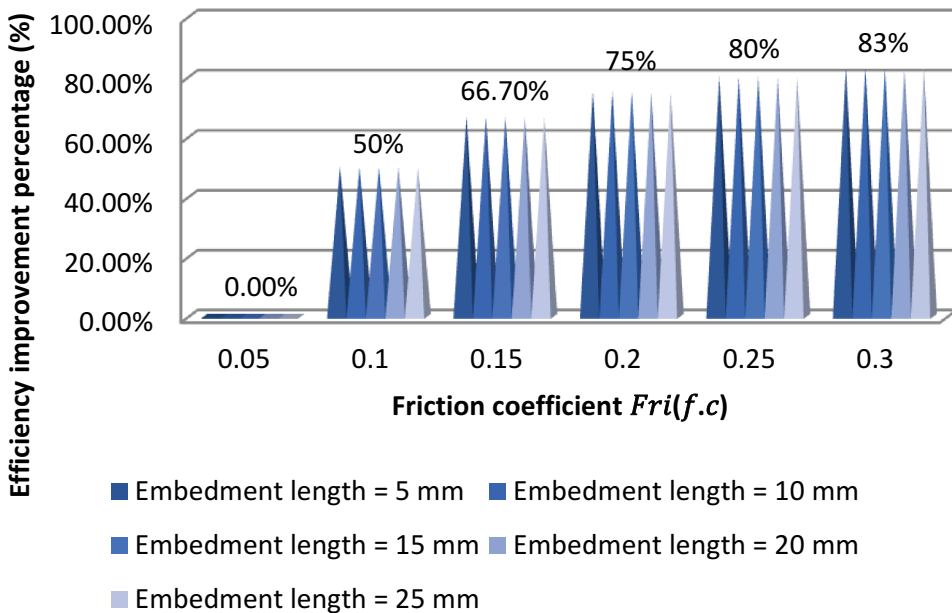


Figure 21. Improvement parentage of frictional-bond strength efficiency.

damage on the concrete surface during the fiber-slip stage, where the collapsed pieces of concrete will be collected on the fiber surface and will fill the roughness spaces, which leads to a smoother sliding between the fiber and the concrete.

4. Conclusions

In this study, the main parameters that may effect the frictional-bond strength between a straight steel fiber-SSF and a concrete matrix have been discussed. At the beginning of this study, the bond-slip mechanism of SSF in cementitious composite was defined.

The relations between the related parameters have been discussed and arranged using new analytical models. Depending on these models, the required equations have been derived. Using the derived equations, the effect of main parameters such as the fiber embedment length, the friction coefficient of fiber/concrete at the interface, the yield strength of the steel fiber, and Poisson's ratio have been discussed. The results of theoretical calculations have been validated by experimental results and numerical simulations as well.

However, the main conclusions of this study can be summarized as the following:

- The frictional-bond strength can be considered as constant versus different values of fiber embedment length.
- Since the full-bond strength was founded by assuming an appropriate length for the steel fiber, to develop its yield strength without failure in the bond between the fiber and the concrete, this means that the plastic elongation of the fiber will not be considered for a bond strength lower than the full-bond strength (such as low values of frictional-bond strength, according to this study experimental records). Therefore, it can be assumed that the plastic elongation of SSF will not be met during the fiber-slip stage in the concrete matrix.
- During the fiber-slip stage, the SSF/concrete-matrix system can be considered as an elastic system, and the stress–displacement relation is semilinear.
- Higher value of fiber/concrete friction coefficient, $Fri_{(f.c)}$, improves the efficiency of the friction-bond strength and improves the performance of SSF/concrete-matrix system against the initial point of fiber sliding.
- The effect of the friction coefficient $Fri_{(f.c)}$ on the efficiency of the frictional-bond strength is limited after exceeding the value of 0.10, and no significant improvements may be expected. This can be interpreted because of the damage on the concrete surface during the fiber-slip stage, where the collapsed pieces of concrete will be collected on the fiber surface and will fill the roughness spaces, which leads to a smoother sliding between the fiber and the concrete.
- Lower interfacial-bond performance is expected in case of using the fiber with a higher yield strength, f_y , where the higher yield strength reduces the impact of friction properties at the interface against fiber/matrix sliding.
- Whatever the value of fiber embedment length, L_{df} , no significant improvements in the surrounding matrix pressure were noticed, with respect to several values of friction coefficient $Fri_{(f.c)}$.

- Increasing the value of friction coefficient, between the fiber and the matrix, improves the interfacial properties of fiber/matrix system by decreasing the required pressure of surrounding concrete to obtain the same value of frictional-bond strength.
- In lightweight concrete, where the content of air voids is high, a higher value of friction coefficient is required to obtain the same frictional-bond strength; consequently, a larger roughness of fiber surface is required.
- Poisson's ratio of concrete does not affect the frictional-bond strength during the sliding stage of fiber, whereas increasing the values of Poisson's ratio of concrete may delay the start time of fiber sliding movement inside the concrete.
- Improving the self-compacting property of fresh concrete may lead to a higher surrounding pressure of concrete matrix; this will shift the tip of debonding zone to be placed at a point versus a greater value of fiber displacement, meaning the partial fiber stretching may add an addition contribution to the frictional-bond strength.

Disclosure statement

No potential conflict of interest was reported by the author(s).

ORCID

Amjad Khabaz  <http://orcid.org/0000-0001-6591-3802>

References

- [1] Hassoun MN, Al-Manaseer A. Structural concrete: theory and design. 6th New Jersey: John Wiley & Sons; 2015.
- [2] Building code requirements for structural concrete (ACI 318-14) and commentary (ACI 318R-14). Farmington Hills MI: American Concrete Institute; 2014.
- [3] En BS. 1-1 eurocode 2: design of concrete structures - Part 1-1: general rules and rules for buildings. Brussels: CEN2004. 1992.
- [4] Khabaz A. Fundamentals of contracts and specifications in civil engineering. Saarbrücken: Scholars' Press. 2016; 978-3-659-84244-3.
- [5] McCormac J, Brown R. Design of reinforced concrete. 10th ed. New Jersey: John Wiley & Sons 2015.
- [6] Bhatt P, MacGinley TJ, Choo BS. Reinforced concrete design to eurocodes: design theory and examples. 4th ed. Boca Raton: CRC Press-Taylor & Francis Group; 2014.
- [7] Calavera J. Manual for detailing reinforced concrete structures to. Vol. EC2. Abingdon: Spon Press-Taylor & Francis Group; 2012.
- [8] Mosley WH, Hulse R, Bungey JH. Reinforced concrete design to eurocode 2. 7th ed. Basingstoke: Palgrave Macmillan; 2012.
- [9] Soetens T, Matthys S. Shear-stress transfer across a crack in steel fibre-reinforced concrete. Cem Concr Compos. 2017;82:1–13.
- [10] Krasnikovs A, Kononova O, Khabaz A, et al. Post-cracking behaviour of high strength fiber concrete prediction and validation. World Acad Sci Eng Technol. 2011;59:988–992.
- [11] Krasnikovs A, Khabaz A, Shahmenko G, et al. Glass and carbon fiber concrete micromechanical and macromechanical properties. Sci J RTU, Transp Eng. 2008;6(28):132–141.
- [12] Krasnikovs A, Khabaz A, Kononova O. Numerical 2d investigation of non-metallic (glass, carbon) fiber micro-mechanical behavior in concrete matrix. Sci J RTU, Construct Sci. 2009;10(10):67–78. 2010.

- [13] Krasnikovs A, Khabaz A, Telnova I I, et al. Numerical 3D investigation of non-metallic (glass, carbon) fiber pull-out micromechanics (in concrete matrix). *Sci J RTU, Transp Eng.* 2010;6(33):103–108.
- [14] Khabaz A. Dynamical analysis of non-metallic (glass, carbon) fiber reinforced concrete under the influence of vibration. *Int J Comp Mater.* 2013;3(6):174–180.
- [15] Borodulina S, Motamedian HR, Kulachenko A. Effect of fiber and bond strength variations on the tensile stiffness and strength of fiber networks. *Int J Solids Struct.* 2018;154:19–32.
- [16] Krasnikovs A, Kononova O, Khabaz A, et al. Fiberconcrete non-linear fracture control through fresh concrete flow numerical simulation. *J Vibro Eng.* 2010;12(2):149–160.
- [17] Khabaz A. Non-metallic fiber reinforced concrete. Saarbrücken: LAP LAMBERT Academic Publishing; 2014; 978-3-659-50914-8.
- [18] Khabaz A. 2D Investigation of bonding forces of straight steel fiber in concrete. *OALib J.* 2015;2:e1991:1–8.
- [19] Zhang W, Xu X, Wang H, et al. Experimental and numerical analysis of interfacial bonding strength of polyoxymethylene reinforced cement composites. *Constr Build Mater.* 2019;207:1–9.
- [20] Le HV, Moon D, Kim DJ. Effects of ageing and storage conditions on the interfacial bond strength of steel fibers in mortars. *Constr Build Mater.* 2018;170:129–141.
- [21] Khabaz A. Construction and design requirements of green buildings' roofs in Saudi Arabia depending on thermal conductivity principle. *Constr Build Mater.* 2018;186:1119–1131.
- [22] Varona FB, Baeza FJ, Bru D, et al. Evolution of the bond strength between reinforcing steel and fibre reinforced concrete after high temperature exposure. *Constr Build Mater.* 2018;176:359–370.
- [23] Kosmatka SH, Wilson ML. Design and control of concrete mixtures, EB001. 15th ed. Skokie Illinois: Portland Cement Association; 2011.
- [24] Mirsayah AA, Banthia N. Shear strength of steel fiber-reinforced concrete. *ACI Mater J.* 2002;99(5):473–479.
- [25] Ali M, Li X, Chouw N. Experimental investigations on bond strength between coconut fibre and concrete. *Mater Des.* 2013;44:596–605.
- [26] Yoo DY, Choi HJ, Kim S. Bond-slip response of novel half-hooked steel fibers in ultra-high-performance concrete. *Constr Build Mater.* 2019;224:743–761.
- [27] Khabaz A. Impact of fiber shape on mechanical behavior of steel fiber in fiber reinforced concrete FRC. *World J Eng Phys Sci.* 2015;3(1):001–006.
- [28] Khabaz A. Monitoring of impact of hooked ends on mechanical behavior of steel fiber in concrete. *Constr Build Mater.* 2016;113:857–863.
- [29] Şahmaran M, Christianto HA, Yaman I. The effect of chemical admixtures and mineral additives on the properties of self-compacting mortars. *Cem Concr Compos.* 2006;28(5):432–440.
- [30] Mpalaskas AC, Vasilakos I, Matikas TE, et al. Monitoring of the fracture mechanisms induced by pull-out and compression in concrete. *Eng Fract Mech.* 2014;128:219–230.
- [31] Li Y, Liu YL, Peng XH, et al. Pull-out simulations on interfacial properties of carbon nanotube-reinforced polymer nanocomposites. *Comput Mater Sci.* 2011;50:1854–1860.
- [32] MdJI A, Lo SR, Karim MR. Pull-out behaviour of steel grid soil reinforcement embedded in silty sand. *Comput Geotech.* 2014;56:216–226.
- [33] Banholzer B, Brameshuber W, Jung W. Analytical simulation of pull-out tests—the direct problem. *Cem Concr Compos.* 2005;27:93–101.
- [34] Shannag MJ, Brincker R, Hansen W. Pullout behavior of steel fibers from cement-based composites. *Cem Concr Res.* 1997;27(6):925–936.
- [35] Khabaz A. Performance evaluation of corrugated steel fiber in cementitious matrix. *Constr Build Mater.* 2016;128:373–383.
- [36] Marshall DB. Analysis of fiber debonding and sliding experiments in brittle matrix composites. *Acta Metall Mater.* 1992;40(3):427–441.
- [37] Khabaz A. Determination of friction coefficient between straight steel fiber and the concrete $fri_{(SSF,C)}$. *Adv Mater.* 2015;4:20–29.

- [38] Khabaz A. Determination of friction coefficient between glass fiber and the concrete $f_{ri(GF,C)}$. *Int J Mater Sci Appl*. 2014;3(6):321–324.
- [39] Yoo DY, Kim S, Kim JJ, et al. An experimental study on pullout and tensile behavior of ultra-high-performance concrete reinforced with various steel fibers. *Construct Build Mater*. 2019;206:46–61.
- [40] Chun B, Yoo DY, Banthia N. Achieving slip-hardening behavior of sanded straight steel fibers in ultra-high-performance concrete. *Cement Concr Compos*. 2020;113:103669.
- [41] Lee Y, Kang ST, Kim JK. Pullout behavior of inclined steel fiber in an ultra-high strength cementitious matrix. *Construct Build Mater*. 2010;24(10):2030–2041.
- [42] Kim JJ, Jang YS, Yoo DY. Tensile properties of ultra-high-performance concrete improved by novel curvilinear steel fibers. *J Mater Res Tech*. 2020;9(4):7570–7582.
- [43] Chatterjee A, Bowling A. Modelling three-dimensional surface-to-surface rigid contact and impact. *Multibody Syst Dyn*. 2019;46(1):1–40.
- [44] Li VC. From micromechanics to structural engineering—the design of cementitious composites for civil engineering applications. *J SCE J Struct Mech Earthquake Engng*. 1993;10(2):37–48.
- [45] Wang Y, Li VC, Backer S. Modeling of fiber pull-out from a cement matrix. *Int J Cement Compos Lightweight Concrete*. 1988;10(3):143–149.
- [46] Shao Y, Li Z, Shah SP. Matrix cracking and interface debonding in fiber reinforced cement-matrix composites. *Adv Cement Based Mater*. 1993;1:55–66.
- [47] Yang JM, Jeng SM, Yang CJ. Fracture mechanisms of fiber-reinforced titanium alloy matrix composites, Part I: interfacial behavior. *Mater Sci Eng*. 1991;138:155–167.
- [48] Bao G, Song Y. Crack bridging models for fiber composites with degraded interfaces. *J Mech Phys Solids*. 1993;41:1425–1444.
- [49] Cox BN, Marshall DB. Stable and unstable solutions for bridged cracks in various specimens. *Acta Metallurgica et Materialia*. 1991;39(4):579–589.
- [50] Khabaz A. Analysis of sliding mechanism of straight steel fibers in concrete and determine the effect of friction. *Arch Civ Mech Eng*. 2017;17(3):599–608.
- [51] Khabaz A. Theoretical analysis and numerical simulation of development length of straight steel fiber in cementitious materials. *Compos Interfaces*. 2017;24(5):447–467.
- [52] Lin Z, Li VC. Crack bridging in fiber reinforced cementitious composites with slip-hardening interfaces. *J Mech Phys Solids*. 1997;45(5):763–787.
- [53] Redon C, Li VC, Wu C, et al. Measuring and modifying interface properties of PVA fibers in ECC matrix. *J Mater Civ Eng*. 2001;13(6):399–406.